AIAA SciTech
5-9 January 2015, Kissimmee, Florida
53rd AIAA Aerospace Sciences Meeting

Numerical modelling of jets exiting from the ASME and conical nozzles

Christophe Bogey* and **Olivier Marsden†**
Laboratoire de Mécanique des Fluides et d'Acoustique
UMR CNRS 5509, Ecole Centrale de Lyon
69134 Ecully, France

Two isothermal round jets at a Mach number of 0.9 and a diameter-based Reynolds number of 2×10^5 have been computed by compressible large-eddy simulation using high-order finite differences on a grid of 3.1 billion points. At the exit of a pipe nozzle in which a trip forcing is applied, they are characterized by flow parameters, including the momentum thickness and the shape factor of the boundary layer, the momentum-thickness-based Reynolds number, and the peak turbulence intensity, which roughly match those found in experiments using two nozzles referred to as the ASME and the conical nozzles. The nozzle-exit boundary layer is therefore in a highly disturbed laminar state in the first jet, and in a turbulent state in the second. The exit flow conditions, the shear-layer and jet flow fields, and the far-field noise provided by the highly-resolved simulations are described and compared. The jet with the ASME-like initial conditions develops a little more rapidly with slightly higher turbulence levels than the other. Overall, however, the results obtained for the two jets are very similar, and they are in good agreement with measurements available for Mach number 0.9 jets. This is in particular true for the far-field pressure spectra. As the ASME nozzle has been reported to yield higher noise levels than the conical nozzle, this suggests that the nozzle-exit conditions of the present jets do not adequately reflect those in the experiments and/or that the link between the noise differences and the jet initial conditions using the two nozzles is not as simple as was first thought.

I. Introduction

Since the work of Crow & Champagne[1] in 1971, it has been well known that the aerodynamic and acoustic characteristics of free shear flows depend on their initial conditions. For subsonic jets, important parameters are the thickness and the shape of the velocity profile, and the turbulence level at the nozzle exit. Their effects on the shear-layer and jet flow fields and the acoustic far field have been described in the 1970s and 1980s by many researchers, including Hill *et al.*,[2] Browand & Latigo,[3] Husain & Hussain,[4] Raman *et al.*,[5,6] Zaman[7,8] and Bridges & Hussain.[9] In particular, it has been established that initially laminar jets develop more rapidly and generate more noise than initially turbulent jets.

In simulations, the issue of the initial conditions is a crucial one, refer to the review papers by Colonius & Lele,[10] Bailly & Bogey,[11] Wang *et al.*[12] and Bodony & Lele.[13] These have been carried out in the late 1990s and early 2000s using both direct numerical simulation (DNS), as in Boersma *et al.*,[14] Stanley & Sarkar[15] and Freund,[16] and large-eddy simulation (LES), as in Zhao *et al.*,[17] Bogey *et al.*[18] and Bodony & Lele.[19] In the simulations of the time, because of the limited computational resources, it was very difficult to prescribe jet initial conditions corresponding to measured conditions, notably in terms of shear-layer thickness.[13] The usual approach was therefore to specify a velocity profile at the inflow, onto which random disturbances or instability modes are added to seed the turbulence. It was the case in the three LES mentioned above, as well as in the studies by Bogey & Bailly[20] and Kim & Choi[21] focusing on the sensitivity to jet initial conditions and forcing. Since then, other approaches have been developed. One possibility is to impose an

*CNRS Research Scientist, AIAA Senior Member & Associate Fellow, christophe.bogey@ec-lyon.fr
†Assistant Professor at Ecole Centrale de Lyon, olivier.marsden@ec-lyon.fr

inflow velocity profile provided by a steady-state computation inside the nozzle, as done in Shur *et al.*[23] Another is to include the final part of the nozzle geometry, e.g. in Andersson *et al.*,[22] or a pipe nozzle, in the computational domain. Following the latter strategy, LES have been run over the past few years by Bogey *et al.*[24–29] for initially laminar and highly disturbed jets at a Mach number of $M = u_j/c_a = 0.9$ and Reynolds numbers $Re_D = u_j D/\nu_j$ between $25,000$ and $Re_D = 200,000$, with laminar exit boundary-layer profiles, where D, u_j, c and ν are the jet diameter and velocity, the speed of sound and the kinematic molecular viscosity, and subscripts j and a denote inflow and ambient conditions. Attempts to compute initially turbulent jets have been made by Bogey *et al.*[30] and Uzun & Hussaini,[31] using a coarse grid in the former case and a grid with a spatial extent limited to 4.5 diameters downstream of the nozzle in the latter. More recently, Sandberg *et al.*[32] performed the simulation of a fully turbulent pipe flow at $Re_D = 7,500$ exiting into a coflow, and Bühler *et al.*[33] successfully computed a jet at $Re_D = 18,100$ with turbulent conditions at the exit of a pipe nozzle. Finally, LES of jets at $Re_D = 50,000$ with thick transitional and turbulent boundary-layer profiles have been carried out in Bogey & Marsden.[34]

In experiments, the question of the initial conditions has received renewed attention since Viswanathan[35]'s claim in 2004 that the jet noise database of Tanna[36] might be contaminated by spurious facility noise. In reply to this, Harper-Bourne[37] suggested that the extra components observed at high frequencies in Tanna[36]'s sound spectra are due to laminar flow conditions at the nozzle exit. This seems to be confirmed by the experimental results acquired by Viswanathan & Clark,[38] Zaman[39] and Karon & Ahuja[40] for jets exiting from the ASME and the conical nozzles of identical exit diameter, differing in internal profile. Indeed, less high-frequency noise is produced using the conical nozzle, which is the nozzle providing the most developed exit boundary layers, as indicated by the measurements by Zaman[39] and Karon & Ahuja[40] for jets over a wide range of Mach numbers. As examples, results obtained just downstream the nozzle by the first author for $M = 0.37$ and nozzles of 1 inch diameter, and by the others for $M = 0.4$ and $D = 1.5$ inches, are provided in table 1. In all cases, the boundary layers are very thin relative to the jet radius $r_0 = D/2$, but they have a larger momentum thickness δ_θ, leading to a higher Reynolds number $Re_\theta = u_j\delta_\theta/\nu_j$, using the conical nozzle. More importantly, they are in a laminar state with the ASME nozzle, but in a turbulent state with the conical nozzle. This is supported, in particular, by the shape factors of $H = \delta^*/\delta_\theta = 2.34$ and 1.71, where δ^* is the boundary-layer displacement thickness, reported by Karon & Ahuja[40] in the two cases. As for the peak axial turbulence intensities u'_e/u_j, where u'_e is the maximum rms value of axial velocity fluctuations near the nozzle exit, they have been found by Zaman[39] to be equal to 11.5% with the ASME nozzle and 7% with the conical nozzle. Thus, the laminar boundary layers from the ASME nozzle appear to be highly disturbed and to contain more velocity fluctuations than the turbulent boundary layers from the conical nozzle, which is counterintuitive and may result in some confusion. Moreover, little is known about the flow fields of the jets. For these reasons, it is interesting to investigate the properties of these jets using numerical simulations.

Table 1. Jet initial conditions in experiments: nozzle type and diameter, Mach number M, Reynolds number Re_D, state, shape factor H and momentum thickness δ_θ of the boundary-layer (BL) profile, Reynolds number Re_θ and peak axial turbulence intensity u'_e/u_j near the nozzle exit. The exit quantities are measured at $z = 0.04r_0$ in Zaman[39] and at $z = 0$ in Karon & Ahuja.[40]

	nozzle	D	M	Re_D	BL state	H	δ_θ/r_0	Re_θ	u'_e/u_j
Zaman[39]	ASME	1 in.	0.37	2.2×10^5	laminar	-	0.0050	556	11.5%
	conical	1 in.	0.37	2.2×10^5	turbulent	-	0.0106	1179	7%
Karon & Ahuja[40]	ASME	1.5 in.	0.40	3.5×10^5	-	2.34	0.0049	870	-
	conical	1.5 in.	0.40	3.5×10^5	-	1.71	0.0065	1135	-

In the present work, two isothermal round jets have been calculated using LES on a grid containing 3.1 billion points using low-dissipation and low-dispersion finite differences and relaxation filtering as subgrid-scale dissipation. The jets have a Mach number $M = 0.9$ and a Reynolds number $Re_D = 2 \times 10^5$. They originate from a $2r_0$-long pipe nozzle, at the inlet of which mean velocity profiles are imposed, and in which a trip-like forcing is employed[25] in order to generate a desired level of turbulent fluctuations at the exit. The inlet velocity profiles and the forcing position and strength have been chosen in order to obtain exit flow conditions, in terms of momentum thickness and the shape factor of the boundary layer, momentum-thickness-based Reynolds number, and peak turbulence intensity, similar to those given in table 1 for the ASME and the conical nozzles. Consequently, the nozzle-exit boundary layer is in a highly disturbed laminar

state in the first jet, and in a turbulent state in the second one. In this work, two objectives are pursued. The first one is to perform the LES of jets with realistic initial conditions at a very high resolution, and to compare the results with available experimental data for laboratory jets at a Mach number of 0.9. The second one is to examine the differences between the flow and acoustic fields of the two jets, and to determine whether they correspond to those measured between the jets from the ASME and the conical nozzles.

The paper is organized as follows. The main characteristics of the different jets and of the simulations, including inflow conditions, numerical methods and computational parameters, are documented in section II. The nozzle-exit flow properties, the mixing-layer and jet flow fields and the jet acoustic fields are described in section III. Concluding remarks are given in section IV. Finally, results from an additional simulation using a finer grid are depicted in the appendix to demonstrate the accuracy of the LES of the jet with a turbulent exit boundary layer.

II. Parameters

A. Jet definition

Two jets, referred to as jetASME and jetConic, are considered. They are isothermal, and have a Mach number of M = 0.9 and a Reynolds number of $\mathrm{Re}_D = 2\times10^5$. The ambient temperature and pressure are $T_a = 293$ K and $p_a = 10^5$ Pa. The jets originate at $z = 0$ from a pipe nozzle of radius r_0 and length $2r_0$, whose lip is $0.05r_0$ thick. At the pipe inlet, different axial velocity profiles are imposed. Radial and azimuthal velocities are set to zero, pressure is equal to p_a, and temperature is determined by a Crocco-Busemann relation. A trip-like forcing is applied to the boundary layers in the pipe, in order to generate disturbed exit conditions for the jets, which otherwise would initially contain only very weak velocity fluctuations. The main parameters of the pipe-inlet axial velocity profiles and of the boundary-layer excitations are collected in table 2. They have been chosen in order to obtain exit boundary-layer conditions similar to those reported in table 1 for the jets of Zaman[39] and Karon & Ahuja,[40] as will be shown later in section III.B.

Table 2. Jet inflow parameters: Mach number M, Reynolds number Re_D, shape factor H, momentum thickness δ_θ and 99% velocity thickness δ_{99} of the boundary-layer profile at the pipe-nozzle inlet, and strength α_{trip} and axial position z_{trip} of the trip-like excitation.

	M	Re_D	H	δ_θ/r_0	δ_{99}/r_0	α_{trip}	z_{trip}
jetASME	0.9	2×10^5	2.55	0.0053	0.037	0.0395	$-0.125r_0$
jetConic	0.9	2×10^5	1.52	0.0117	0.104	0.0231	$-0.35r_0$

The inlet axial velocity profiles are represented in figure 1(a). In jetASME, the profile is a Blasius laminar boundary-layer profile with a shape factor H = 2.55, given by the Pohlhausen's fourth-order polynomial approximation

$$\frac{u_{inlet}(r)}{u_j} = \begin{cases} \dfrac{(r_0-r)}{\delta_{BL}}\left[2-2\left(\dfrac{(r_0-r)}{\delta_{BL}}\right)^2+\left(\dfrac{r_0-r}{\delta_{BL}}\right)^3\right] & \text{if} \quad r \geq r_0-\delta_{BL} \\ 1 \quad \text{otherwise} \end{cases} \tag{1}$$

with $\delta_{BL} = 0.0045r_0$, yielding a momentum thickness of $\delta_\theta = 0.0053r_0$ and a 99% velocity thickness of $\delta_{99} = 0.037r_0$. In jetConic, the inlet velocity profile is transitional boundary-layer profile[34] with H = 1.52 defined as

$$\frac{u_{inlet}(r)}{u_j} = \begin{cases} \left(\sin\left[\dfrac{\pi}{2}\left(\dfrac{r_0-r}{\delta_{T_2}}\right)^{\beta_2}\right]\right)^{\gamma_2} & \text{if} \quad r \geq r_0-\delta_{T_2} \\ 1 \quad \text{otherwise} \end{cases} \tag{2}$$

where $\beta_2 = 0.423$, $\gamma_2 = 0.82$ and $\delta_{T_2} = 0.1328r_0$, leading to $\delta_\theta = 0.0117r_0$ and $\delta_{99} = 0.104r_0$. This profile has been designed to fit the experimental data obtained by Schubauer & Klebanoff[41] in a flat-plate boundary layer in the region of changeover from laminar to fully turbulent conditions, refer to the appendix A of a recent paper.[34]

The two jets are 'tripped' as is usually done in laboratory experiments for boundary layers over a flat plate or in jet nozzles, e.g. in Klebanoff & Diehl[42] and Crow & Champagne,[1] using an arbitrary tripping

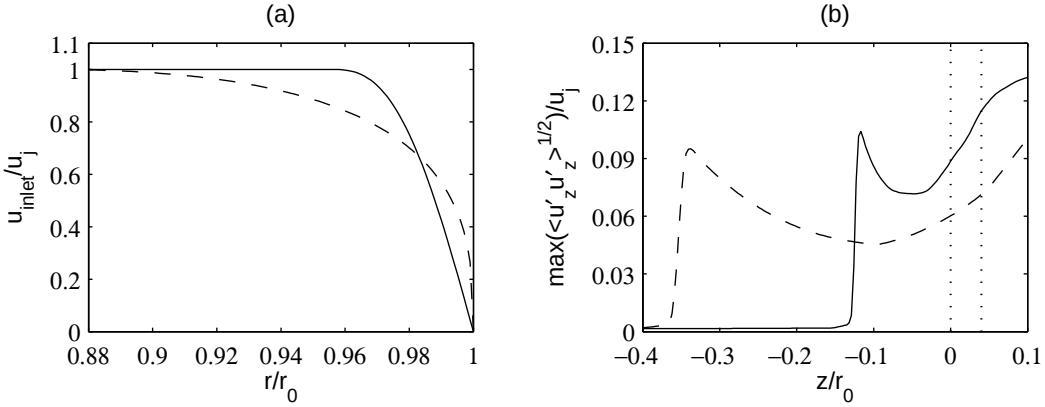

Figure 1. Representation (a) of the axial velocity profile u_{inlet} imposed at the pipe-nozzle inlet and (b) of the peak rms value of axial velocity fluctuations u'_z: ——— jetASME, − − − jetConic; ····· $z = 0$ and $z = 0.04$.

device.[42–47] The forcing procedure detailed in the appendix A of Bogey *et al.*[25] is implemented in the present jets. It consists in adding random low-level vortical disturbances uncorrelated in the azimuthal direction in the boundary layers, and has been previously applied to both laminar[25–29] and non-laminar[34] velocity profiles. The position and the strength of the forcing are indicated in table 2. They have been adjusted in order to reach peak turbulence intensities of about 11.5% in jetASME and 7% in jetConic at $z = 0.04r_0$ close to the nozzle exit as in the jets of Zaman[39] considered in table 1. This point is illustrated in figure 1(b) showing the variations of the maximum rms value of axial velocity fluctuations in the pipe and just downstream. On the basis of previous studies and preliminary tests, the forcing is located at $z_{trip} = -0.125r_0$ in jetASME and $z_{trip} = -0.35r_0$ in jetConic, and the values of the coefficient α_{trip} specifying the forcing strength are set to 0.046 and 0.095, respectively. Finally, pressure fluctuations of maximum amplitude 200 Pa, random in both space and time, are added in the shear layers between $z = 0.25r_0$ and $z = 4r_0$ from $t = 0$ up to non-dimensional time $t = 12.5r_0/u_j$, in order to speed up the initial transient period.

B. LES procedure and numerical methods

The LES are carried out using a solver of the three-dimensional filtered compressible Navier-Stokes equations in cylindrical coordinates (r, θ, z) based on low-dissipation and low-dispersion explicit schemes. The axis singularity is taken into account by the method of Mohseni & Colonius.[48] In order to alleviate the time-step restriction near the cylindrical origin, the derivatives in the azimuthal direction around the axis are calculated at coarser resolutions than permitted by the grid.[49] For the points closest to the jet axis, the effective azimuthal discretization is thus equal to $2\pi/32$. Fourth-order eleven-point centered finite differences are used for spatial discretization, and a second-order six-stage Runge-Kutta algorithm is implemented for time integration.[50] A twelfth-order thirteen-point centered filter[51] is applied explicitly to the flow variables every time step. Non-centered finite differences and filters are also used near the pipe walls and the grid boundaries.[24,52] The radiation conditions of Tam & Dong[53] are applied at all boundaries, with the addition at the outflow of a sponge zone combining grid stretching and Laplacian filtering.[54]

The explicit filtering is employed to remove grid-to-grid oscillations, but also as a subgrid high-order dissipation model in order to relax turbulent energy from scales at wave numbers close to the grid cut-off wave number while leaving larger scales mostly unaffected.[55–58] In order to check this point, and to assess the reliability of the present LES, the transfer functions associated with molecular viscosity, relaxation filtering and time integration are compared as proposed in Bogey *et al.*[25] They are evaluated for the minimum and maximum mesh spacings in the jets, namely the radial mesh spacing at $r = r_0$ and the axial mesh spacing at $z \geq 25r_0$. They are presented in figures 2(a,b) according to the normalized wave number $k\Delta$, where Δ is the mesh spacing. For $\Delta = \Delta r(r = r_0)$, in figure 2(a), the transfer function of molecular viscosity is found to be higher than that of the relaxation filtering for wave numbers $k\Delta < 1.52$, corresponding to wavelengths $\lambda/\Delta > 4.13$, and inversely lower for $k\Delta > 1.52$ and $\lambda/\Delta < 4.13$. A similar behavior is noticed in figure 2(b) for $\Delta = \Delta z(z \geq 25r_0)$. Here, the two dissipation functions intersect at $k\Delta = 0.49$, that is for $\lambda/\Delta = 12.72$ points per wavelength. In both figures, in addition, the transfer function of time integration is well below

that of viscosity for all wave numbers. These results indicate that the largest turbulent structures in the LES are mainly dissipated by molecular viscosity. The physics of these structures is therefore unlikely to be governed by either numerical or subgrid-modeling dissipation. This should allow the effective flow Reynolds number not to be artificially decreased, and viscosity effects to be captured, as was the case in a previous study.[28]

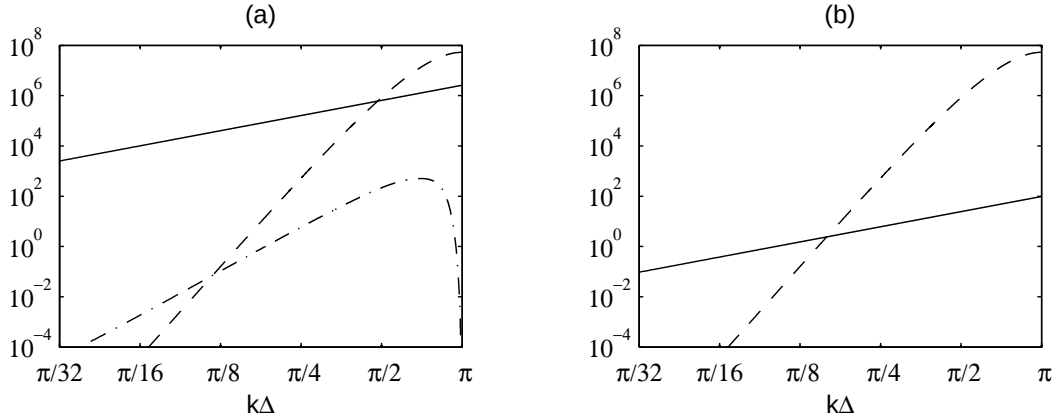

Figure 2. Representation of the dissipation functions associated with ——— molecular viscosity, − − − relaxation filtering, and − · − · time integration, according to normalized wave number $k\Delta$ for (a) $\Delta = \Delta r(r = r_0) = 0.0015r_0$, and (b) $\Delta = \Delta z(z \geq 25r_0) = 0.025r_0$.

C. Simulation parameters

As mentioned in table 3, the LES grid contains $n_r \times n_\theta \times n_z = 496 \times 2048 \times 3052 = 3.1$ billion points. There are 393 points along the pipe nozzle between $z = -2r_0$ and $z = 0$, and 151 points between $r = 0$ and $r = r_0$. The physical domain extends axially down to $L_z = 28.4r_0$, and radially out to $L_r = 8.4r_0$.

Table 3. Grid parameters: numbers of points n_r, n_θ and n_z in the radial, azimuthal and axial directions, extents L_r and L_z of the physical domain, and mesh spacings Δr and Δz at different positions.

					$\Delta r/r_0$ (%) at $r =$				$\Delta z/r_0$ (%) at $z =$			
n_r	n_θ	n_z	L_r	L_z	0	r_0	$2r_0$	$4r_0$	0	$5r_0$	$15r_0$	$25r_0$
487	2048	3052	$8.4r_0$	$28.4r_0$	1.54	0.15	1.83	5	0.31	0.74	1.62	2.5

The mesh spacings are uniform in the azimuthal direction, yielding $r\Delta\theta/r_0 = 0.31\%$ at $r = r_0$, but vary in the radial and axial directions, as shown in figures 3(a,b). In the radial direction, the mesh spacing is minimum at $r = r_0$, where $\Delta r/r_0 = 0.15\%$. On both sides of the nozzle lip line, it increases at a rate of 1.68% to reach $\Delta r/r_0 = 1.5\%$ at $r = 0$ on the jet axis, and $\Delta r/r_0 = 5\%$ at $r = 3.9r_0$. Beyond $r = 3.9r_0$, the mesh spacing is constant up to $r = L_r = 8.4r_0$, and then grows again up to a value of $\Delta r/r_0 = 17.6\%$. This allows the radial boundary of the computational domain to be pushed back to $r = 14r_0$. In the axial direction, the mesh spacing is minimum between $z = -r_0$ and $z = 0$, where $\Delta z/r_0 = 0.31\%$. It increases upstream of $z = -r_0$, but also downstream of the nozzle exit at a rate of 0.087% up to $z = 25r_0$. The mesh spacing is thus equal to $\Delta z/r_0 = 2.5\%$ between $z = 25r_0$ and $z = L_z = 28.4r_0$. Further downstream, a 120-point sponge zone is applied using a grid stretching rate of 4.2%.

The LES grid has been built using 3.1 billion points with attention paid to obtaining very fine discretization everywhere in the jet in the three spatial directions, see for instance the radial and axial mesh spacings provided in table 3. The minimum mesh spacings of $\Delta r/r_0 = 0.15\%$, $r_0\Delta\theta/r_0 = 0.31\%$ and $\Delta z/r_0 = 0.31\%$ have specifically been chosen in order to compute the thin boundary layers and shear layers of the jets properly. These values have been set based on previous results obtained for Mach number 0.9 jets using similar numerical methods and a grid with minimum mesh spacings of $\Delta r/r_0 = 0.36\%$, $r_0\Delta\theta/r_0 = 0.61\%$ and $\Delta z/r_0 = 0.72\%$, which are about two times larger than those in the present grid. In an early study, in particular, a jet with a laminar, highly disturbed boundary layer, characterized by $\delta_{BL} = 0.09r_0$ at the pipe-nozzle inlet and $\mathrm{Re}_\theta = 487$ and $u'_e/u_j = 9.13\%$ at the exit, was simulated. The flow properties downstream

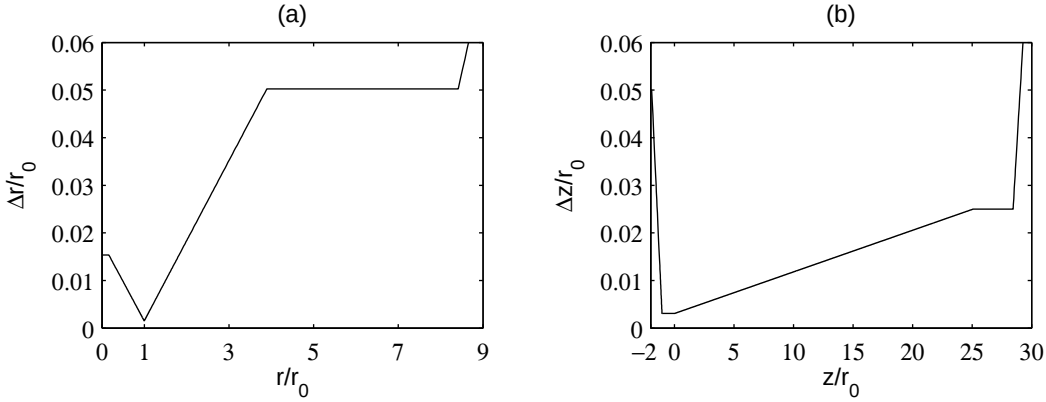

Figure 3. Representation of the radial and axial mesh spacings: (a) $\Delta r/r_0$, and (b) $\Delta z/r_0$.

of the nozzle were found to be independent of the grid.[29] Consequently, the grid resolution can be expected to be appropriate in the jetASME case exhibiting a laminar inlet boundary-layer profiles with $\delta_{BL} = 0.045r_0$, and $\mathrm{Re}_\theta = 580$ and $u'_e/u_j = 8.86\%$ at the nozzle exit, as will be reported in section III.B.

Regarding the jetConic case with an inlet transitional boundary-layer profile of thickness $\delta_{T_2} = 0.1328r_0$ and exit parameters of $\mathrm{Re}_\theta = 1100$ and $u'_e/u_j = 6.02\%$, see also in section III.B, it can first be noted that a jet with $\delta_{T_2} = 0.332r_0$, $\mathrm{Re}_\theta = 691$ and $u'_e/u_j = 6.14\%$ was recently calculated successfully on the grid mentioned above.[34] In jetConic, the near-wall mesh spacings in the pipe expressed in wall units based on the wall friction velocity at the nozzle exit, given in table 4, are equal to $\Delta r^+ = 3.7$, $(r_0\Delta\theta)^+ = 7.4$ and $\Delta z^+ = 7.4$. The azimuthal and axial mesh spacings are therefore sufficient, because they meet the requirements needed to compute turbulent wall-bounded flows accurately, using direct numerical simulation as in Kim *et al.*[59] and Spalart[60] for instance, or using LES involving relaxation filtering as in Gloerfelt & Berland[61] and Kremer & Bogey.[58] For the wall-normal spacing, an additional LES has been performed using a finer grid. For $z \leq 3.5r_0$, this grid is identical to the first grid in the directions θ and z, but differs in the radial direction with $\Delta r/r_0 = 0.08\%$ instead of $\Delta r/r_0 = 0.15\%$ at $r = r_0$. In the new LES, moreover, the tripping procedure is exactly the same as in the first LES, and the time step is halved because of the CFL stability condition, leading to an application of the relaxation filtering that is twice as frequent. The flow fields obtained using the two grids at the nozzle exit and in the mixing layers developing further downstream have very similar features, as illustrated in the appendix. This demonstrates that the LES solutions do not depend significantly on the radial mesh spacing at $r = r_0$ or on the relaxation filtering.

Table 4. Near-wall mesh spacings Δr, $r_0\Delta\theta$ and Δz given in wall units based on the wall friction velocity at the nozzle exit.

	Δr^+	$(r_0\Delta\theta)^+$	Δz^+
jetASME	3.0	6.0	6.0
jetConic	3.7	7.4	7.4

The LES have run on 1024 processors of a distributed memory cluster using a hybrid MPI-OpenMP in-house solver, and consumed about 2 million CPU hours. A total of 271,300 iterations have been performed in each case, leading to a simulation time of $320r_0/u_j$. After the initial transient period, density, velocity components and pressure are recorded from time $t = 94r_0/u_j$ onwards, on the jet axis and on two surfaces at $r = r_0$ and $r = r_c = 7.5r_0$, at a sampling frequency allowing the computation of spectra up to a Strouhal number $\mathrm{St}_D = fD/u_j = 20$, where f is the time frequency. The cylindrical surface surrounding the jets is located at $r = 7.5r_0$, in a region where the radial mesh spacing yields a Strouhal number $\mathrm{St}_D = 11.1$ for an acoustic wave discretized by four points per wavelength. In the azimuthal direction, every second grid point is stored, allowing data post-processing to be performed up to the azimuthal mode $n_\theta = 1024$, where n_θ is the dimensionless azimuthal wave number such that $n_\theta = k_\theta r$. The velocity spectra are evaluated from overlapping samples of duration $27.4r_0/u_j$. The flow statistics are determined from $t = 175r_0/u_j$ onwards, and they are averaged in the azimuthal direction. They can be considered to be well converged in view of the results obtained at intermediary stages of the LES for $t \geq 300r_0/u_j$.

D. Far-field extrapolation

The LES near fields of jetASME and jetConic have been propagated to the acoustic far field by solving the isentropic linearized Euler equations in cylindrical coordinates.[62] The extrapolation is performed from fluctuating velocities and pressure recorded in the LES on a surface at $r = 7.5r_0$ as mentioned above. These data are interpolated onto a cylindrical surface discretized by an axial mesh spacing of $\Delta z = 0.05r_0$. They are then imposed at the bottom boundary of the grid on which the ILEE are solved using the same numerical methods as in the LES. This grid contains $n_r \times n_\theta \times n_z = 2090 \times 512 \times 2000 = 2.3$ billion points, and extends axially from $z = -34r_0$ up to $z = 94r_0$ and radially up to $r = 122r_0$. For $-2r_0 \leq z \leq 94r_0$, the radial and axial mesh spacings are uniform with $\Delta r = \Delta z = 0.05r_0$, yielding $\mathrm{St}_D = 11$ for an acoustic wave at four points per wavelength. After a time $t \simeq 120r_0/u_j$, pressure is recorded at a distance of $120r_0$ from $z = r = 0$ where far-field acoustic conditions are expected to apply according to experiments,[63,64] for angles relative to the jet direction between $\phi = 40^\circ$ and $\phi = 90^\circ$, during a period of about $200r_0/u_j$. Pressure spectra are evaluated using overlapping samples of duration $38r_0/u_j$, and they are averaged in the azimuthal direction.

III. Results

A. Vorticity and pressure snapshots

Snapshots of the vorticity norm obtained in the vicinity of the nozzle exit between $z = -0.4r_0$ and $z = -1.2r_0$, and in the shear layers up to $z = 15r_0$, are represented in figures 4(a,b) and 5(a,b), respectively. In the first figures, the boundary-layer tripping due to the forcing at $z_{trip} = -0.125r_0$ in jetASME and $z_{trip} = -0.35r_0$ in jetConic is clearly visible. High levels of vorticity are found immediately downstream of the nozzle very near the lip line. As expected given the inlet boundary-layer thicknesses, they spread over a larger radial extent in jetConic than in jetASME. The region of changeover from boundary-layer to mixing-layer flow conditions also appears to be longer in the axial direction in jetConic. In that jet, the shear layer shows turbulent structures elongated in the streamwise direction, typical of wall-bounded flows, close to the nozzle, then it rolls up around $z = 0.4r_0$, and is visually fully developed for about $z \geq r_0$. Further downstream, in figures 5(a,b), the mixing layers look quite similar in the two cases, and exhibit large-scale structures resembling the coherent structures revealed by the flow visualizations of Brown & Roshko.[65]

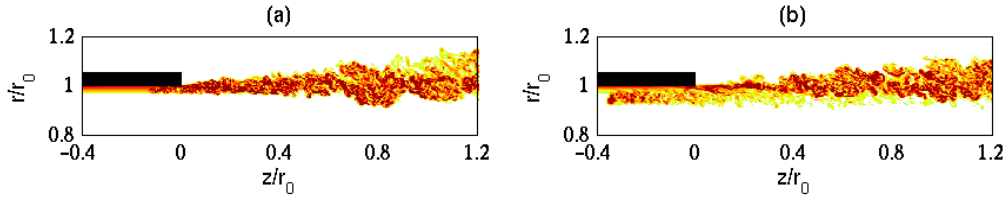

Figure 4. Snapshots in the (z, r) plane of vorticity norm $|\omega|$ for (a) jetASME, and (b) jetConic. The color scale ranges up to the level of $48u_j/r_0$.

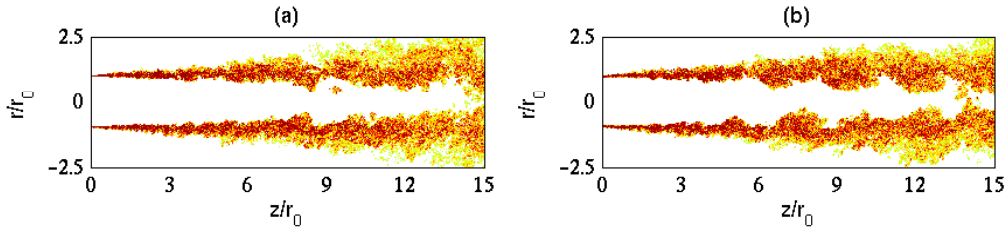

Figure 5. Snapshots in the (z, r) plane of vorticity norm $|\omega|$ for (a) jetASME, and (b) jetConic. The color scale ranges up to the level of $14u_j/r_0$.

Snapshots of the vorticity norm and of the pressure field obtained down to $z = 28r_0$ simultaneously inside and outside the jets by LES are provided in figures 6(a,b). The results in the two cases do not seem to be fundamentally different from each other. Both jets indeed exhibit a potential core ending around $z = 16r_0$, and large-scale near-field pressure fluctuations. The latter are classically associated with the flow coherent structures, and have been discussed in Arndt *et al.*[66] and Coiffet *et al.*[67] for instance.

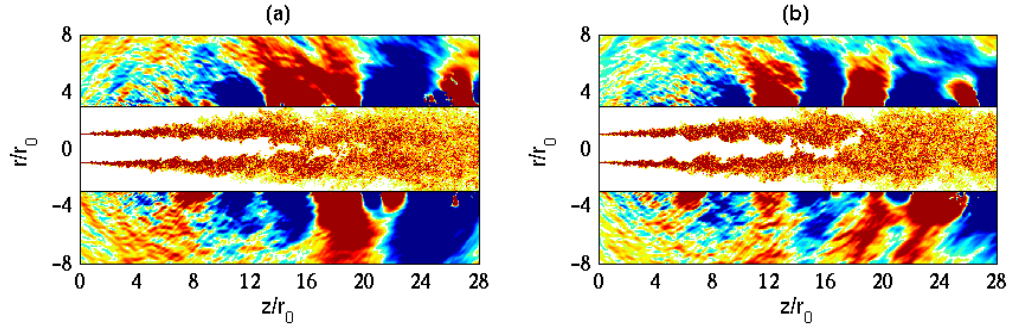

Figure 6. Snapshots in the (z, r) plane of vorticity norm $|\omega|$ in the jet and of pressure fluctuations $p - p_a$ outside for (a) jetASME, and (b) jetConic. The color scales range up to the level of $8u_j/r_0$ for vorticity, and from −80 to 80 Pa for pressure.

Finally, snapshots of the pressure fields computed up to a distance of $120r_0$ to the nozzle exit from the LES data at $r = 7.5r_0$ by solving the isentropic linearized Euler equations are displayed in figures 7(a,b). For both jets, low-frequency acoustic components characterized by wavelengths $\lambda \simeq 15r_0$, yielding Strouhal numbers $\mathrm{St}_D \simeq 0.15$, are dominant for small angles relative to the flow direction, which does not seem to be the case in the sideline direction. This is in agreement with the experimental observations of Mollo-Christensen *et al.*,[68] Lush[69] and Tam *et al.*,[70] among others. Acoustic waves at very low Strouhal numbers are also noted, especially in the jetASME case. They are most likely to be spurious waves caused by the presence of aerodynamic fluctuations at the end of the LES surface used for the far-field wave extrapolations. Fortunately, they do not appear to affect the far-field spectra for Strouhal numbers $\mathrm{St}_D \geq 0.1$ for radiation angles $\phi \leq 75^\circ$ with respect to the jet axis, as will be shown in section III.E.

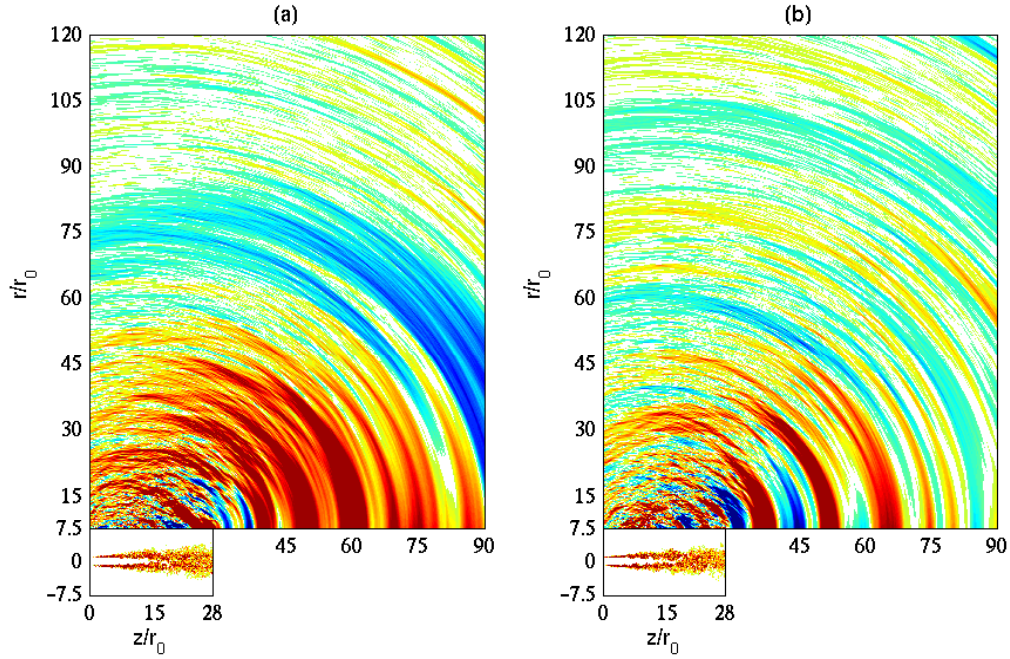

Figure 7. Snapshots in the (z, r) plane of vorticity norm $|\omega|$ in the jet and of pressure fluctuations $p - p_a$ outside for (a) jetASME, and (b) jetConic. The color scales range up to the level of $8u_j/r_0$ for vorticity, and from −28 to 28 Pa for pressure.

B. Nozzle-exit conditions

The profiles of mean and rms axial velocities calculated at the nozzle exit of jetASME and jetConic are presented in figures 8(a,b), and the main exit flow parameters are provided in table 5. As intended, the exit

boundary-layer profiles differ significantly in figure 8(a). Their shape factors are equal to H = 2.44 and 1.88, their momentum thicknesses are $\delta_\theta = 0.0058 r_0$ and $0.0111 r_0$, yielding $\mathrm{Re}_\theta = 580$ and 1110, and their 99% velocity thicknesses are $\delta_{99} = 0.041 r_0$ and $0.102 r_0$. The values of H, δ_θ / r_0 and Re_θ in jetASME and jetConic are in line with the measurements of Zaman[39] and Karon & Ahuja[40] for jets from the ASME and the conical nozzles, respectively, in table 1. The boundary-layer profile in the first jet corresponds to a laminar profile, and, given that H $\simeq$ 1.45 is obtained[44,45,60,71] for fully developed boundary layers at $\mathrm{Re}_\theta \simeq 1000$, the profile in the second jet is transitional. As for the radial distributions of the rms values of velocity fluctuations in figure 8(b), they also vary, and reach peak values u'_e/u_j of 8.86% at $r_e = 0.992 r_0$ in jetASME and of 6.02% at $r_e = 0.985 r_0$ in jetConic. Therefore, the jet with a laminar exit velocity profile is initially more disturbed than the jet with a non-laminar profile, which seems contradictory, but happens sometimes as pointed out by Raman *et al.*[5]

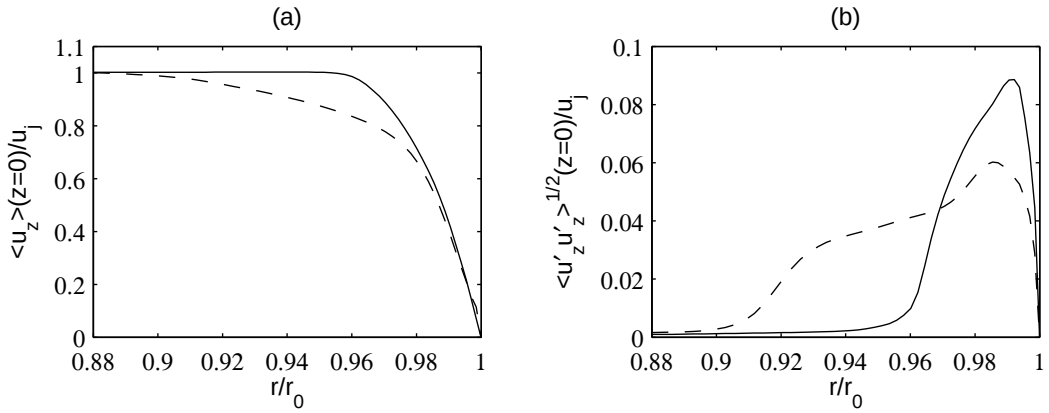

Figure 8. Radial profiles at the nozzle exit (a) of mean axial velocity $< u_z >$ and (b) of the rms values of axial velocity fluctuations u'_z: ——— jetASME, − − − jetConic.

Table 5. Nozzle-exit parameters: shape factor H, momentum thickness δ_θ and 99% velocity thickness δ_{99} of the boundary-layer profile, Reynolds number $\mathrm{Re}_\theta = u_j \delta_\theta / \nu$, value u'_e/u_j and radial position r_e of peak axial turbulence intensity, and peak azimuthal mode n_θ at $r = r_e$.

	H	δ_θ/r_0	δ_{99}/r_0	Re_θ	u'_e/u_j	r_e/r_0	n_θ
jetASME	2.44	0.0058	0.041	580	8.86%	0.992	203
jetConic	1.88	0.0111	0.102	1110	6.02%	0.985	135

Spectra of axial velocity fluctuations are evaluated at the nozzle exit at the position $r = r_e$ of the turbulence intensity peak. They are represented as a function of the Strouhal number St_D in figure 9(a), and of the azimuthal mode n_θ in figure 9(b). The levels are higher in the spectra of jetASME than in jetConic, which is not surprising in view of the maximum rms values u'_e/u_j in the two jets. The shapes of the spectra are roughly the same in the two cases, and correspond, as was discussed in a note[26] on that matter, to the spectral shapes encountered for turbulent wall-bounded flows because of the presence of large-scale elongated structures.[72] The relative magnitude of the high-frequency components appears however stronger in the spectra of JetASME with a thinner boundary layer. The flat region observed for low Strouhal numbers in figure 9(a) thus extends up to $\mathrm{St}_D \simeq 2.5$ in jetConic, but to $\mathrm{St}_D \simeq 5$ in jetASME. The dominant components in figure 9(b) also shift towards higher modes, resulting in peaks at $n_\theta = 135$ in jetConic and at $n_\theta = 203$ in jetASME, as reported in table 5. At the location of peak turbulence level, the turbulent structures are consequently spaced out by $\lambda_\theta = 0.047 r_0$ and $\lambda_\theta = 0.031 r_0$, respectively. They are well discretized by the grid using mesh spacings of $0.0031 r_0$ at $r = r_0$ in the azimuthal direction.

C. Shear-layer development

The variations over $0 \leq z \leq 15 r_0$ of the momentum thickness δ_θ and of the spreading rate $\mathrm{d}\delta_\theta/\mathrm{d}z$ of the mixing layers are presented in figures 10(a,b). In figure 10(a), the shear-layer developments in the two jets turn out not to be significantly different, and to agree fairly well with that measured by Fleury *et al.*[73] in

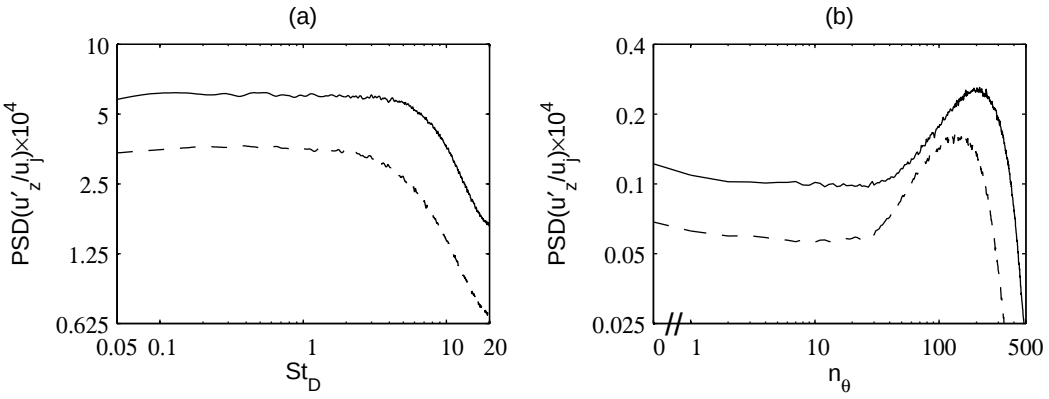

Figure 9. Power spectral densities (PSD) of axial velocity fluctuations u'_z obtained at the nozzle exit at the position $r = r_e$ of peak axial turbulence intensity, as functions (a) of Strouhal number $\mathrm{St}_D = fD/u_j$ and (b) of azimuthal mode n_θ: ——— jetASME, − − − jetConic.

an isothermal jet at M = 0.9 and $\mathrm{Re}_D = 7.7 \times 10^5$. It is a little faster in jetASME than in jetConic, leading to slightly higher values of spreading rates in figure 10(b) for the former jet. The curves in that figure both exhibit a double-hump shape. They first grow rapidly with the axial distance just downstream of the nozzle to reach peak values of 0.27 at $z = 0.1r_0$ in jetASME and of 0.26 at $z = 0.4r_0$ in jetConic, and then decrease by about 20%. For $z \geq 1.5r_0$, they increase again, but more slowly than previously, up to $z = 10.2r_0$ in jetASME and to $z = 12r_0$ in jetConic, where they achieve values of around 0.27. These results look very much like those obtained experimentally by Husain & Hussain[4] for initially turbulent axisymmetric mixing layers. Farther downstream, the spreading rates diminish as the end of the potential core is approached.

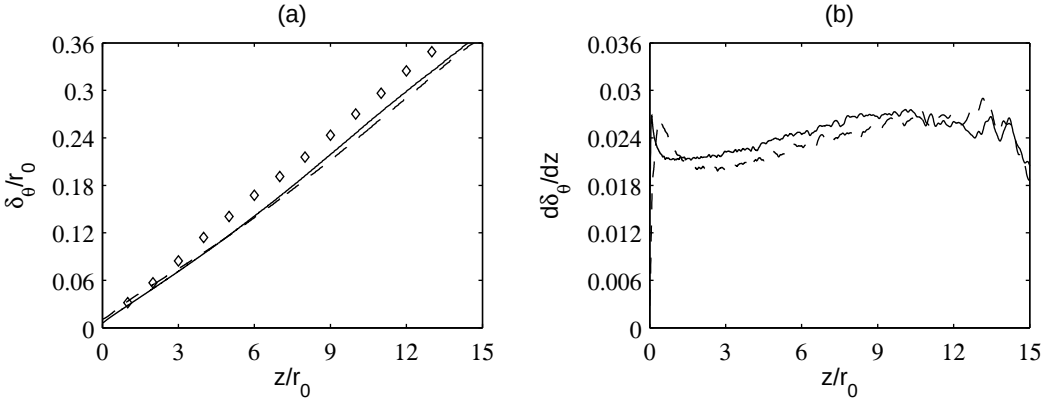

Figure 10. Variations (a) of shear-layer momentum thickness δ_θ and (b) of spreading rate $\mathrm{d}\delta_\theta/\mathrm{d}z$: ——— jetASME, − − − jetConic; ◇ measurements of Fleury *et al.*[73] for a Mach number 0.9 jet.

The peak rms values of axial and radial velocity fluctuations estimated between $z = 0$ and $z = 15r_0$ are displayed in figures 11(a,b). Their streamwise evolutions in the two jets are very similar, showing a rapid growth downstream of the nozzle, a small hump near $z = r_0$, then a very slow increase nearly up to $z = 15r_0$. They agree well with the experimental data obtained by Fleury[74] and Castelain[75] for isothermal, Mach number 0.9 jets at $\mathrm{Re}_D = 7.7 \times 10^5$ and $\mathrm{Re}_D = 10^6$ using Particle Image Velocimetry (PIV). The discrepancy in figure 11(b) with respect to Fleury[74]'s data is probably due to an underestimation of the turbulence values by the PIV method, which occurred in other jet experiments according to Bridges & Wernet.[76] The rms levels of velocity fluctuations are slightly higher in jetASME than in jetConic. At $z = 6r_0$, for instance, they are equal to 16.4% and 15.9% for u'_z, and of 11.5% and 11.1% for u'_r, respectively. The maximum turbulence intensities, provided in table 6, are however almost identical in the two jets. In particular, a peak value of 16.8% is found for the axial velocity fluctuations in both cases. This value is comparable to those measured by Husain & Hussain[4] in the similarity region of initially turbulent axisymmetric mixing layers.

The spectra of radial velocity fluctuations calculated on the lip line at the two axial locations $z = 0.2r_0$

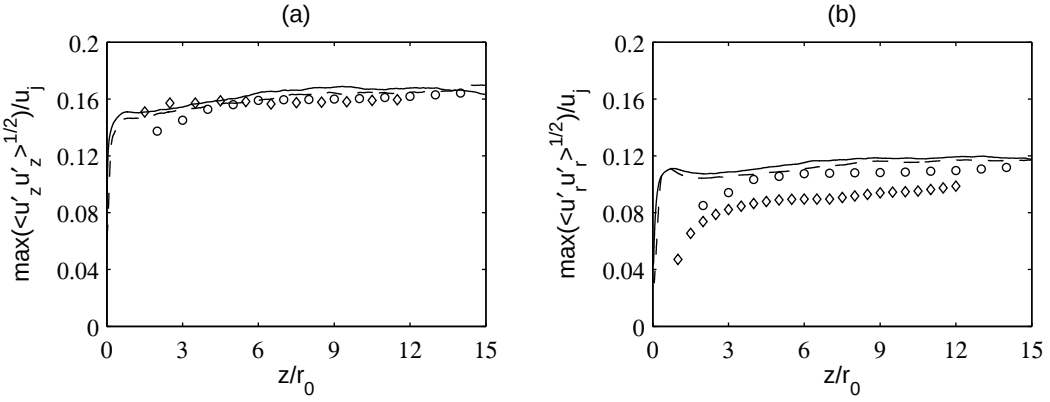

Figure 11. Variations of the peak rms values of (a) axial and (b) radial velocity fluctuations u'_z and u'_r: ——— jetASME, − − − jetConic; measurements for Mach number 0.9 jets: ◇ Fleury,[74] ○ Castelain.[75]

Table 6. Peak turbulence intensities in the jets, and Strouhal numbers St_D and $\mathrm{St}_\theta = f\delta_\theta(z=0)/u_j$ given by the peak frequency in the spectra of radial velocity fluctuations at $z = 0.2r_0$ and $r = r_0$.

	$<u'^2_z>^{1/2}/u_j$	$<u'^2_r>^{1/2}/u_j$	$<u'^2_\theta>^{1/2}/u_j$	$<u'_r u'_z>^{1/2}/u_j$	St_D	St_θ
jetASME	16.8%	11.9%	13.8%	9.6%	4.5	0.013
jetConic	16.8%	12%	13.6%	9.4%	4.8	0.027

and $z = 6r_0$ are presented in figures 12(a,b) as a function of the Strouhal number St_D. At the first location very near the nozzle, in figure 12(a), an instability-like component appears to emerge in both jets. This component is centered around $\mathrm{St}_D = 4.5$ in jetASME and $\mathrm{St}_D = 4.8$ in jetConic, yielding Strouhal numbers based on the nozzle-exit momentum thickness of $\mathrm{St}_\theta = 0.013$ and $\mathrm{St}_\theta = 0.027$ as reported in table 6. Therefore, the peak frequency obtained in jetASME with a laminar boundary-layer profile falls within the range of frequencies predominating early on in initially laminar mixing layers according to linear stability analyses[77] and experiments.[78] For jetConic with a transitional profile, it moves out of this range. The same trend was observed for jets with thicker boundary-layer profiles in Bogey & Marsden.[34] In particular, a peak frequency at $\mathrm{St}_\theta = 0.026$ was initially found in a jet with a nozzle-inlet profile given by equation (2) as in jetConic. Further downstream at $z = 6r_0$, in figure 12(b), the radial velocity spectra in the two jets display very similar broadband shapes and amplitudes over the whole range of frequencies considered.

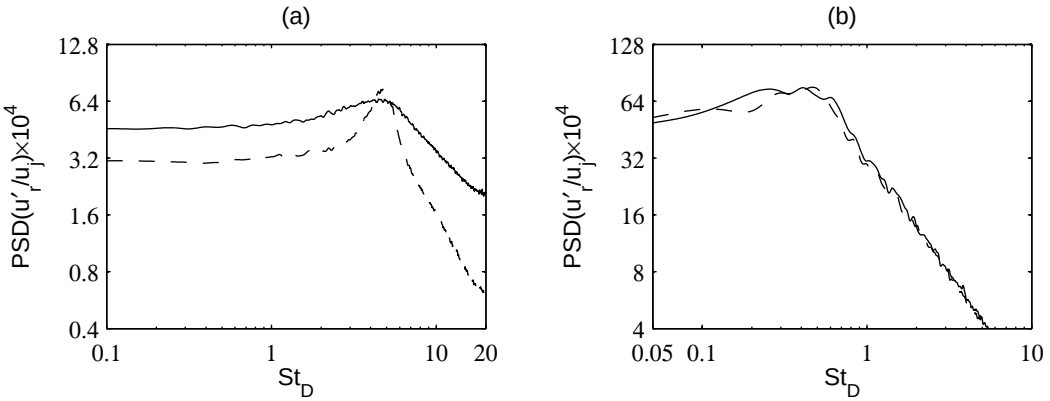

Figure 12. Power spectral densities (PSD) of radial velocity fluctuations u'_r (a) at $z = 0.2r_0$ and $r = r_0$ and (b) at $z = 6r_0$ and $r = r_0$, as functions of St_D: ——— jetASME, − − − jetConic.

D. Jet development

The variations of the centerline mean axial velocity and of the jet half-width $\delta_{0.5}$, given by the radial position at which the mean velocity is equal to half of its centerline value, are presented in figures 13(a,b). The curves obtained for the two jets are nearly superimposed, but also reveal that the development of jetASME is slightly more rapid than that of jetConic, which is consistent with the differences in shear-layer spreading rate noted in the previous section. This leads to potential cores ending respectively at $z_c = 15.3r_0$ and $z_c = 15.6r_0$, as indicated in table 7, with z_c being defined as the axial distance at which the centerline mean velocity is equal to $0.95u_j$. Furthermore, the LES profiles compare well with the experimental data available for four jets at a Mach number of 0.9 and Reynolds numbers $\mathrm{Re}_D \geq 5 \times 10^5$, namely the cold jet of Bridges,[81] the isothermal jets of Lau *et al.*[79] and Fleury *et al.*,[73] and the slightly heated jet of Arakeri *et al.*[80] More precisely, they lie in the middle of the measurement points in figure 13(a), and pass through the points of Fleury *et al.*[73] in figure 13(b).

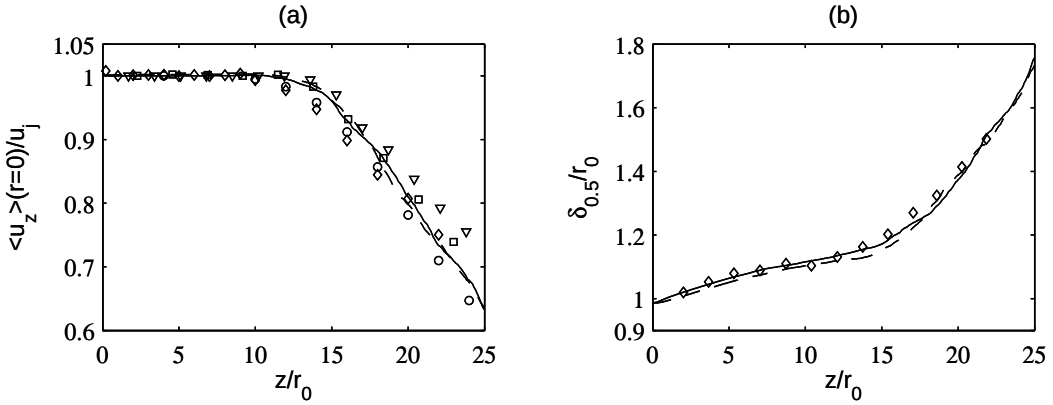

Figure 13. Variations (a) of mean axial velocity $< u_z >$ on the jet axis and (b) of jet velocity half-width $\delta_{0.5}$: ——— jetASME, − − − jetConic; measurements for Mach number 0.9 jets: ○ Lau *et al.*,[79] □ Arakeri *et al.*,[80] ▽ Bridges,[81] ◇ Fleury *et al.*[73]

Table 7. Axial position of the end of the potential core z_c, where $u_c(z_c) = 0.95u_j$, and peak rms values of velocity fluctuations u'_z and u'_r on the jet axis.

	z_c/r_0	$<u_z'^2>^{1/2}/u_j$	$<u_r'^2>^{1/2}/u_j$
jetASME	15.3	15%	11.6%
jetConic	15.6	14.8%	11.2%

The variations of the centerline rms values of axial and radial velocity fluctuations are shown in figures 14(a,b). As is the case for the mean flow profiles, the results are very similar in jetASME and jetConic. In both jets, the peak turbulence intensities are reached around $z = 21r_0$, and are equal to about 15% for velocity u'_z and 11.5% for velocity u'_r, see in table 7 for the exact values. Compared to the experiments on Mach number 0.9 jets mentioned above, there is a good agreement with the data of Lau *et al.*[79] and Bridges.[81] The fluctuation levels obtained by Fleury *et al.*[73] and especially by Arakeri *et al.*[80] by performing PIV measurements are significantly lower. As pointed out in section II.C. after having seen the discrepancies in maximum radial turbulence intensities in figure 11(b), this seems to be a frequent issue when the PIV technique is applied to jet flows.[76]

For completeness, the spectra of axial velocity fluctuations calculated at $z = 15.5r_0$, that is close to the end of the potential core in both jets, on the jet axis and on the nozzle lip line, are presented in figures 15(a,b) as a function of the Strouhal number St_D. The spectra at $r = 0$ are less smooth than those at $r = 0.5r_0$ because, unlike the latter, they cannot be averaged in the azimuthal direction. Despite this, the spectra obtained in jetASME and jetConic do not appear to differ much over the entire frequency range. They also strongly resemble the experimental spectra presented in Bridges & Wernet[82] for a cold, 51 mm diameter jet at a Mach number of 0.9.

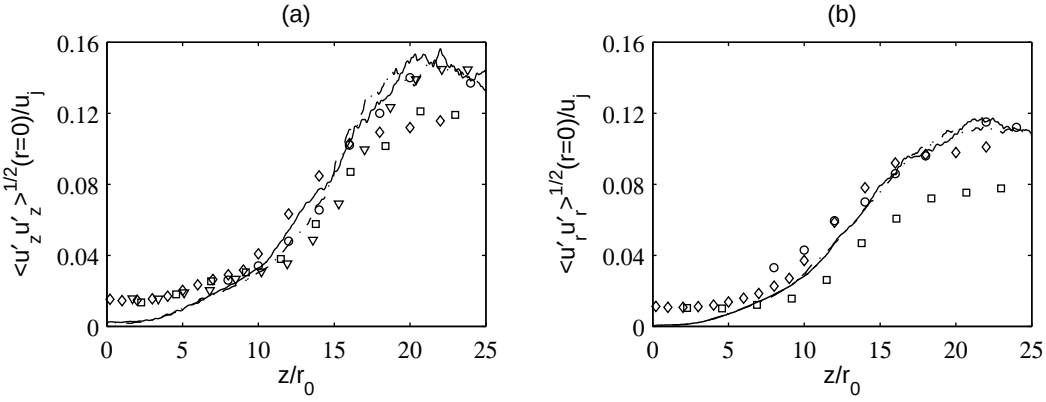

Figure 14. Variations of the centerline rms values of (a) axial and (b) radial velocity fluctuations u'_z and u'_r: ——— jetASME, − − − jetConic; measurements for Mach number 0.9 jets: ○ Lau *et al.*,[79] □ Arakeri *et al.*,[80] ▽ Bridges,[81] ◇ Fleury *et al.*[73]

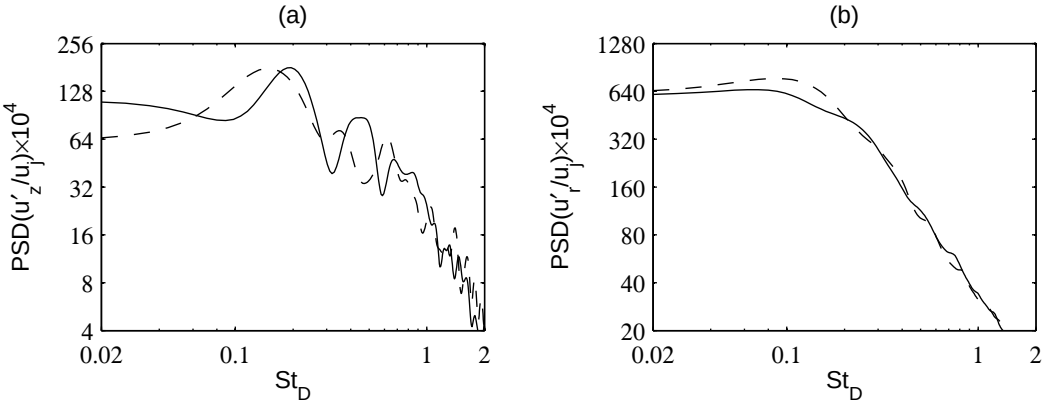

Figure 15. Power spectral densities (PSD) of axial velocity fluctuations u'_z (a) at $z = 15.5r_0$ and $r = 0$ and (b) at $z = 15.5r_0$ and $r = r_0$, as functions of St_D: ——— jetASME, − − − jetConic.

E. Acoustic fields

Far-field spectra determined for jetASME and jetConic from the pressure signals obtained at 120 radii from the nozzle exit from the LES near field by solving the isentropic linearized Euler equations are now displayed. The spectra computed at the radiation angles of $\phi = 40^o$ and $\phi = 75^o$ relative to the jet direction are represented in figures 16(a,b) as a function of the Strouhal number St_D. It appears that for both angles and for all frequencies, the noise levels from jetASME and jetConic are very close. In addition, they agree very well with the spectra acquired by Bridges & Brown[83] for an isothermal jet at $\mathrm{M} = 0.9$ and $\mathrm{Re}_D = 10^6$ at 150 radii from the nozzle exit, scaled to the distance of 120 radii. This experimental data set was chosen among many others, because it has been proved not to be contaminated by extra sound sources, which could result from laminar upstream flow conditions for example. The spectra obtained for the present jets at $\phi = 90^o$ are not shown, because they are dominated by spurious components for $\mathrm{St}_D \leq 0.2$, as mentioned in section III.A and illustrated in figure 7(a). However, as for the spectra at $\phi = 40^o$ and $\phi = 75^o$, they are nearly superimposed and fit the measurements of Bridges & Brown[83] for $\mathrm{St}_D \geq 0.2$.

Given that the differences in turbulence intensities between the two jets are small both in the shear layers and on the jet axis in figures 11 and 13, it is not surprising that the jets generate similar noise levels. In particular, the jetASME simulation does not reproduce the noise increase observed for Strouhal numbers $\mathrm{St}_D \geq 0.4$ at all radiation angles in the experiments of Viswanathan & Clark,[38] Zaman[39] and Karon & Ahuja[40] with the ASME nozzle. The reasons for this are for the moment unclear. A possibility is that the nozzle-exit conditions in the LES, and particularly in jetASME, do not correspond satisfactorily to the jet initial conditions in the experiments. One can wonder especially whether the use of a nozzle pipe instead of the full nozzle geometry is sufficient, and whether the jets with laminar boundary layers from the ASME

nozzle really contain about 10% of rms velocity fluctuations at the nozzle exit. Another possibility, which does not exclude the first, is that the discrepancies in high-frequency noise between the ASME and the conical nozzles do not only result from the laminar and turbulent states of the exit boundary layers, but that other parameters, associated with the nozzle internal geometry for instance, also play an important role.

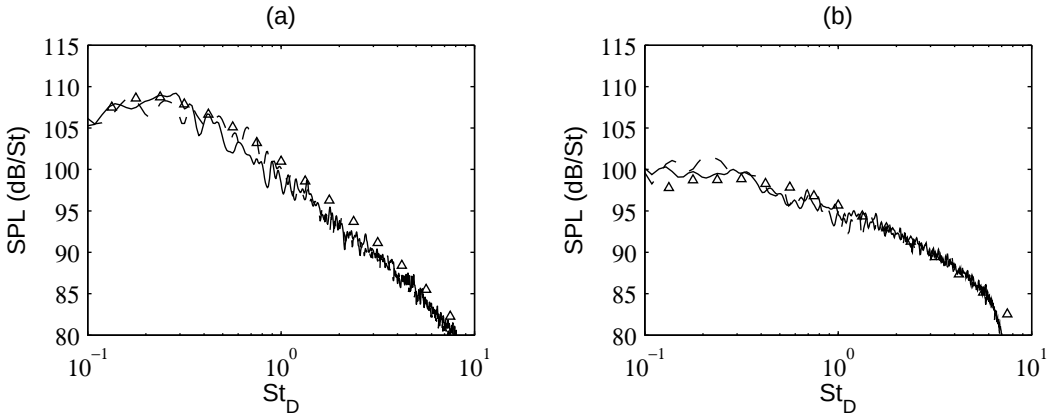

Figure 16. Sound pressure levels (SPL) obtained at a distance of $120r_0$ from the nozzle exit for the angles (a) $\phi = 40^o$ and (b) $\phi = 75^o$ relative to the jet direction, as a function of St_D: ——— jetASME, − − − jetConic; ▽ measurements of Bridges & Brown[83] for an isothermal, Mach number 0.9 jet.

IV. Conclusion

Two isothermal round jets at a Mach number of M = 0.9 and a Reynolds number of $Re_D = 2 \times 10^5$, have been simulated using a very fine grid of 3.1 billion points. They exit from a pipe nozzle with flow conditions, including the momentum thickness and the shape factor of the boundary layer, the momentum-thickness-based Reynolds number, and the peak turbulence intensity, similar to those obtained in experiments for jets from the ASME and the conical nozzles. Thus, the nozzle-exit boundary layer is in a highly disturbed laminar state in the ASME case, and in a turbulent state in the conical case. The flow properties at the nozzle exit, in the shear layers and on the jet centerline, as well as the far-field noise radiated by the two jets, have been investigated. The jet with the ASME-like initial conditions is found to contain more high-frequency velocity fluctuations at the nozzle exit than the other jet, which is most likely due to its thinner boundary layer. Its mixing layers also develop a little more rapidly, leading to a shorter potential core, with slightly higher turbulence intensities. The differences between the two cases are however small, and the flow and sound field of both jets are in good agreement with available experimental data for jets at M = 0.9 and $Re_D \geq 5 \times 10^5$. Finally, no extra noise components are noted for the jet with the ASME-like upstream conditions, contrarily to what is observed in experiments with the ASME nozzle. Further experimental and numerical work is required to identify the reasons for this. In particular, additional measurements of the flow characteristics at the nozzle exit and in the shear layers for jets from the ASME nozzle would be very useful.

Appendix

In order to investigate the sensitivity of the LES results to the near-wall mesh spacing, a simulation of jetConic has been performed on a grid finer than the grid defined in table 3. This new grid is limited to $z = 3.5r_0$ in the axial direction to save computational time. For $z \leq 3.5r_0$, it is identical to the other one in the directions θ and z, but differ in the direction r with a mesh spacing $\Delta r/r_0 = 0.08\%$ instead of $\Delta r/r_0 = 0.15\%$ at $r = r_0$. In the additional LES, the tripping procedure is exactly the same as in the LES using the first grid, and the time step is halved because of the CFL stability condition, leading to an application of the relaxation filtering that is twice as frequent. The flow properties obtained using the two grids at the nozzle exit and in the mixing layers are found to be very similar. Consequently, they depend neither on the wall-normal spacing, nor on the explicit filtering applied to remove grid-to-grid oscillations as well as to relax subgrid-scale turbulent energy.

By way of illustration, some results are represented below, including vorticity snapshots in figures 17(a,b), the radial profiles at the nozzle-exit of mean axial velocity and of turbulence intensities using outer units in figures 18(a,b) and wall units 19(a,b), and the variations of the shear-layer momentum thickness and of the peak turbulence intensities in figures 20(a,b). In the last three figures, the solutions calculated with the reference grid (in black) and with the finer grid (in grey) superpose or are very close to each other.

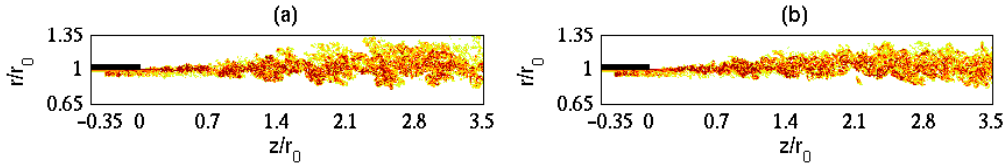

Figure 17. Snapshots in the (z, r) plane of vorticity norm $|\omega|$ obtained for jetConic using (a) the reference grid defined in table 3 and (b) a finer grid with $\Delta r/r_0 = 0.08\%$ instead of $\Delta r/r_0 = 0.15\%$ at $r = r_0$. The color scale ranges up to the level of $40u_j/r_0$,

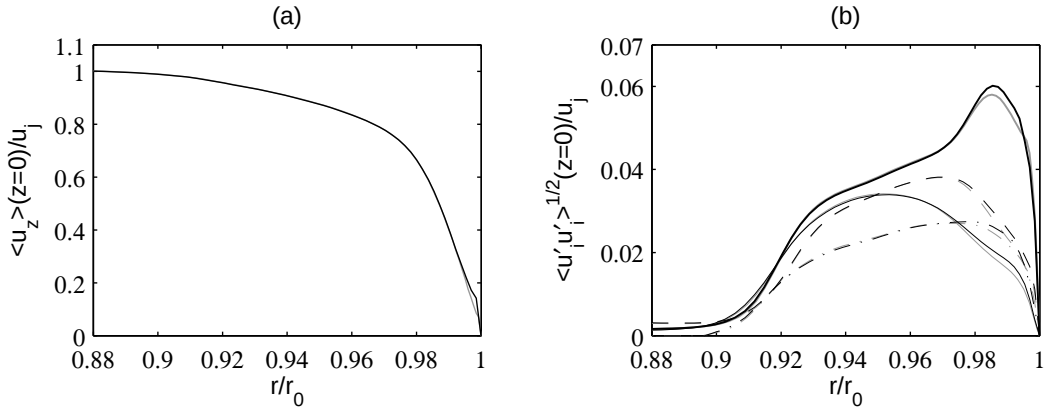

Figure 18. Radial profiles at the nozzle exit (a) of mean axial velocity $< u_z >$ and (b) of turbulence intensities $\_\_\_\_\_$ $< u_z'^2 >^{1/2}/u_j$, $\_\_\_\_\_$ $< u_r'^2 >^{1/2}/u_j$, $- - -$ $< u_\theta'^2 >^{1/2}/u_j$ and $- \cdot - \cdot -$ $< u_r'u_z' >^{1/2}/u_j$ obtained for jetConic using (black) the reference grid and (grey) the finer grid.

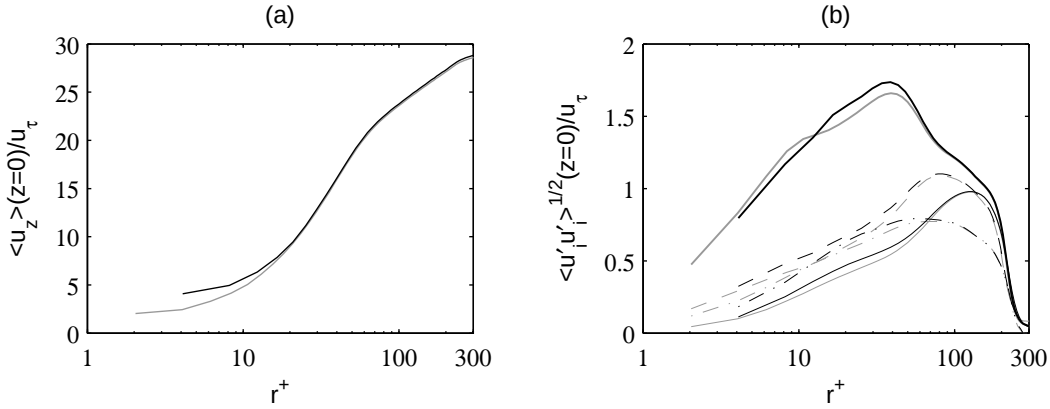

Figure 19. Radial profiles at the nozzle exit (a) of mean axial velocity and (b) of turbulence intensities, represented in wall units based on the wall friction velocity using the same linetypes as in figure 18.

Acknowledgments

This work was granted access to the HPC resources of TGCC (Très Grand Centre de calcul du CEA), CINES (Centre Informatique National de l'Enseignement Supérieur) and IDRIS (Institut du Développement et des Ressources en Informatique Scientifique) under the allocation 2014-2a0204 made by GENCI (Grand

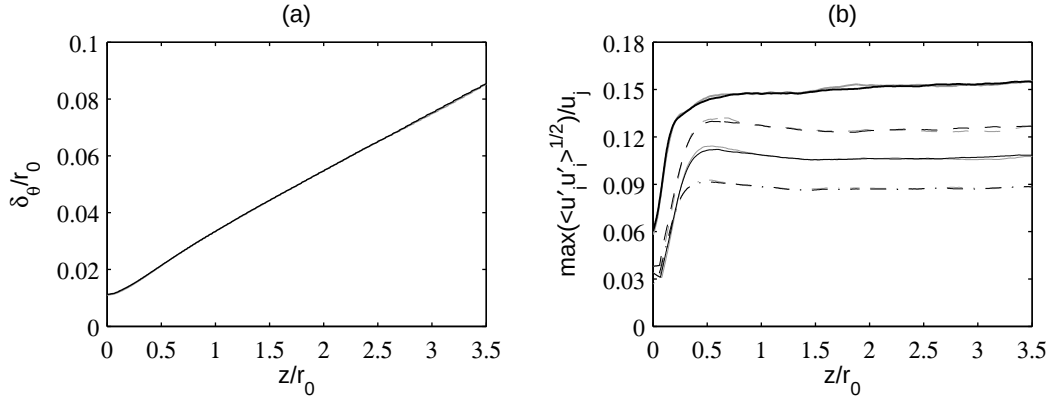

Figure 20. Variations (a) of shear-layer momentum thickness δ_θ and (b) the peak values of turbulence intensities ——— $< u_z'^2 >^{1/2} /u_j$, ——— $< u_r'^2 >^{1/2} /u_j$, − − − $< u_\theta'^2 >^{1/2} /u_j$ and − · − · $< u_r'u_z' >^{1/2} /u_j$ obtained for jetConic using (black) the reference grid and (grey) the finer grid.

Equipement National de Calcul Intensif).

References

[1]Crow, S.C. and Champagne, F.H., "Orderly structure in jet turbulence," *J. Fluid Mech.*, Vol. 48, 1971, pp. 547-591.

[2]Hill, W.G., Jenkins, R.C., and Gilbert, B.L., "Effects of the initial boundary-layer state on turbulent jet mixing," *AIAA J.*, Vol. 14, No. 11, 1976, pp. 1513-1514.

[3]Browand, F.K. and Latigo, B.O., "Growth of the two-dimensional mixing layer from a turbulent and nonturbulent boundary layer," *Phys. Fluids*, Vol. 22, No. 6, 1979, pp. 1011-1019.

[4]Husain, Z.D. and Hussain, A.K.M.F., "Axisymmetric mixing layer: influence of the initial and boundary conditions," *AIAA J.*, Vol. 17, No. 1, 1979, pp. 48-55.

[5]Raman, G., Zaman, K.B.M.Q., and Rice, E.J., "Initial turbulence effect on jet evolution with and without tonal excitation," *Phys. Fluids A*, Vol. 1, No. 7, 1989, pp. 1240-1248.

[6]Raman, G., Rice, E.J., and Reshotko, E., "Mode spectra of natural disturbances in a circular jet and the effect of acoustic forcing," *Exp. Fluids*, Vol. 17, 1994, pp. 415-426.

[7]Zaman, K.B.M.Q., "Effect of initial condition on subsonic jet noise," *AIAA J.*, Vol. 23, 1985, pp. 1370-1373.

[8]Zaman, K.B.M.Q., "Far-field noise of a subsonic jet under controlled excitation," *J. Fluid Mech.*, Vol. 152, 1985, pp. 83-111.

[9]Bridges, J.E. and Hussain, A.K.M.F., "Roles of initial conditions and vortex pairing in jet noise," *J. Sound Vib.*, Vol. 117, No. 2, 1987, pp. 289-311.

[10]Colonius, T. and Lele, S.K., "Computational aeroacoustics: progress on nonlinear problems of sound generation," *Progress in Aerospace Sciences*, Vol. 40, 2004, pp. 345-416.

[11]Bailly, C. and Bogey, C., "Contributions of CAA to jet noise research and prediction," *Int. J. Comput. Fluid Dyn.*, Vol. 18, No. 6, 2004, pp. 481-491.

[12]Wang, M., Freund, J.B., and Lele, S.K., "Computational prediction of flow-generated sound," *Annu. Rev. Fluid. Mech.*, Vol. 38, 2006, pp. 483-512.

[13]Bodony, D.J. and Lele, S.K., "On the current status of jet noise predictions using large-eddy simulation," *AIAA J.*, Vol. 46, No. 2, 2008, pp. 364-380.

[14]Boersma, B.J., Brethouwer, G., and Nieuwstadt, F.T.M., "A numerical investigation on the effect of the inflow conditions on the the self-similar region of a round jet," *Phys. Fluids*, Vol. 10, No 4, 1998, pp. 899909.

[15]Stanley, S.A. and Sarkar, S., "Influence of nozzle conditions and discrete forcing on turbulent planar jets," *AIAA J.*, Vol. 38, No. 9, 2000, pp. 1615-1623.

[16]Freund, J.B., "Noise sources in a low-Reynolds-number turbulent jet at Mach 0.9," *J. Fluid Mech.*, Vol. 438, 2001, pp. 277-305.

[17]Zhao, W., Frankel, S.H., and Mongeau, L., "Large eddy simulations of sound radiation from subsonic turbulent jets," *AIAA J.*, Vol. 39, No. 8, 2001, pp. 1469-1477.

[18]Bogey, C., Bailly, C., and Juvé, D., "Noise investigation of a high subsonic, moderate Reynolds number jet using a compressible LES," *Theoret. Comput. Fluid Dynamics*, Vol. 16, No. 4, 2003, pp. 273-297.

[19]Bodony, D.J. and Lele, S.K., "On using large-eddy simulation for the prediction of noise from cold and heated turbulent jets," *Phys. Fluids*, Vol. 17, No. 8, 2005, 085103.

[20]Bogey, C. and Bailly, C., "Effects of inflow conditions and forcing on a Mach 0.9 jet and its radiated noise," *AIAA J.*, Vol. 43, No. 5, 2005, pp. 1000-1007.

[21]Kim, J. and Choi, H., "Large eddy simulation of a circular jet: effect of inflow conditions on the near field," *J. Fluid Mech.*, Vol. 620, 2009, pp. 383-411.

[22]Andersson, N., Eriksson, L.-E., and Davidson, L., "Large-eddy simulation of subsonic turbulent jets and their radiated sound," *AIAA J.*, Vol. 43, No. 9, 2005, pp. 1899-1912.

[23]Shur, M.L., Spalart, P.R. and Strelets, M.Kh., "LES-based evaluation of a microjet noise reduction concept in static and flight conditions," *J. Sound Vib.*, Vol. 330, No. 17, 2011, pp. 4083-4097.

[24]Bogey, C. and Bailly, C., "Influence of nozzle-exit boundary-layer conditions on the flow and acoustic fields of initially laminar jets," *J. Fluid Mech.*, Vol. 663, 2010, pp. 507-539.

[25]Bogey, C., Marsden, O., and Bailly, C., "Large-Eddy Simulation of the flow and acoustic fields of a Reynolds number 10^5 subsonic jet with tripped exit boundary layers," *Phys. Fluids*, Vol. 23, No. 3, 2011, 035104.

[26]Bogey, C., Marsden, O., and Bailly, C., "On the spectra of nozzle-exit velocity disturbances in initially nominally turbulent jets," *Phys. Fluids*, Vol. 23, No. 9, 2011, 091702.

[27]Bogey, C., Marsden, O., and Bailly, C., "Influence of initial turbulence level on the flow and sound fields of a subsonic jet at a diameter-based Reynolds number of 10^5," *J. Fluid Mech.*, Vol. 701, 2012, pp. 352-385.

[28]Bogey, C., Marsden, O., and Bailly, C., "Effects of moderate Reynolds numbers on subsonic round jets with highly disturbed nozzle-exit boundary layers," *Phys. Fluids*, Vol. 24, No. 10, 2012, 105107.

[29]Bogey, C. and Marsden, O., "Identification of the effects of the nozzle-exit boundary-layer thickness and its corresponding Reynolds number in initially highly disturbed subsonic jets," *Phys. Fluids*, Vol. 25, No. 5, 2013, 055106.

[30]Bogey, C., Barré, S., and Bailly, C., "Direct computation of the noise generated by subsonic jets originating from a straight pipe nozzle," *Int. J. Aeroacoust.*, Vol. 7, No. 1, 2008, pp. 1-22.

[31]Uzun, A. and Hussaini, M., "Investigation of high frequency noise generation in the near-nozzle region of a jet using large eddy simulation," *Theoret. Comput. Fluid Dynamics*, Vol. 21, No. 4, 2007, pp. 291-321.

[32]Sandberg, R.D., Sandham, N.D., and Suponitsky, V., "DNS of compressible pipe flow exiting into a coflow," *Int. J. Heat and Fluid Flow*, Vol. 35, 2012, pp. 33-44.

[33]Bühler, S., Kleiser, L., and Bogey, C., "Simulation of subsonic turbulent nozzle-jet flow and its near-field sound," *AIAA J.*, Vol. 52, No. 8, 2014, pp. 1653-1669.

[34]Bogey, C. and Marsden, O., "Influence of nozzle-exit boundary-layer profile on high-subsonic jets," AIAA Paper 2014-2600, 2014.

[35]Viswanathan, K., "Aeroacoustics of hot jets," *J. Fluid Mech.*, Vol. 516, 2004, pp. 39-82.

[36]Tanna, H.K., "An experimental study of jet noise. Part I: Turbulent mixing noise," *J. Sound Vib.*, Vol. 50, No. 3, 1977, pp. 405-428.

[37]Harper-Bourne, M., "Jet noise measurements: past and present," *Int. J. Aeroacoust.*, Vol. 9, No. 4 & 5, 2010, pp. 559-588.

[38]Viswanathan, K. and Clark, L.T., "Effect of nozzle internal contour on jet aeroacoustics," *Int. J. Aeroacoust.*, Vol. 3, No. 2, 2004, pp. 103-135.

[39]Zaman, K.B.M.Q., "Effect of initial boundary-layer state on subsonic jet noise," *AIAA J.*, Vol. 50, No. 8, 2012, pp. 1784-1795.

[40]Karon, A.Z. and Ahuja, K.K., "Effect of nozzle-exit boundary layer on jet noise," AIAA Paper 2013-0615, 2013.

[41]Schubauer, G.B. and Klebanoff, P.S., "Contributions on the mechanics of boundary-layer transition," NACA TN-3498, 1955.

[42]Klebanoff, P.S. and Diehl, Z.W., "Some features of artificially thickened fully developed turbulent boundary layers with zero pressure gradient," NACA TN-1110, 1952.

[43]Coles, D.E., "The turbulent boundary layer in a compressible fluid," Rand. Rep. R-403-PR, 1962.

[44]Erm, P.L. and Joubert, P.N, "Low-Reynolds-number turbulent boundary layers," *J. Fluid Mech.*, Vol. 230, 1991, pp. 1-44.

[45]Schlatter, P and Örlü, R., "Turbulent boundary layers at moderate Reynolds numbers: inflow length and tripping effects," *J. Fluid Mech.*, Vol. 710, 2012, pp. 5-34.

[46]Hutchings, N., "Caution: tripping hazards," *J. Fluid Mech.*, Vol. 710, 2012, pp. 1-4.

[47]Castillo, L. and Johansson, T.G., "The effects of the upstream conditions on a low Reynolds number turbulent boundary layer with zero pressure gradient," *J. Turbulence*, Vol. 3, 2012, 031.

[48]Mohseni, K. and Colonius, T., "Numerical treatment of polar coordinate singularities," *J. Comput. Phys.*, Vol. 157, No. 2, 2000, pp. 787-795.

[49]Bogey, C., de Cacqueray, N., and Bailly, C., "Finite differences for coarse azimuthal discretization and for reduction of effective resolution near origin of cylindrical flow equations," *J. Comput. Phys.*, Vol. 230, No. 4, 2011, pp. 1134-1146.

[50]Bogey, C. and Bailly, C., "A family of low dispersive and low dissipative explicit schemes for flow and noise computations," *J. Comput. Phys.*, Vol. 194, No. 1, 2004, pp. 194-214.

[51]Bogey, C., de Cacqueray, N., and Bailly, C., "A shock-capturing methodology based on adaptative spatial filtering for high-order non-linear computations," *J. Comput. Phys.*, Vol. 228, No. 5, 2009, pp. 1447-1465.

[52]Berland, J., Bogey, C., Marsden, O., and Bailly, C., "High-order, low dispersive and low dissipative explicit schemes for multi-scale and boundary problems," *J. Comput. Phys.*, Vol. 224, No. 2, 2007, pp. 637-662.

[53]Tam, C.K.W and Dong, Z., "Radiation and outflow boundary conditions for direct computation of acoustic and flow disturbances in a nonuniform mean flow., *J. Comput. Acoust.*, Vol. 4, No. 2,, 1996, pp. 175-201.

[54]Bogey, C. and Bailly, C., "Three-dimensional non reflective boundary conditions for acoustic simulations: far-field formulation and validation test cases," *Acta Acustica*, Vol. 88, No. 4, 2002, pp. 463-471.

[55]Bogey, C. and Bailly, C., "Large Eddy Simulations of transitional round jets: influence of the Reynolds number on flow development and energy dissipation," *Phys. Fluids*, Vol. 18, No. 6, 2006, 065101.

[56]Bogey, C. and Bailly, C., "Turbulence and energy budget in a self-preserving round jet: direct evaluation using large-eddy simulation," *J. Fluid Mech.*, Vol. 627, 2009, pp. 129-160.

[57]Fauconnier, D., Bogey, C., and Dick, E., "On the performance of relaxation filtering for large-eddy simulation," *J. Turbulence*, Vol. 14, No. 1, 2013, pp. 22-49.

[58]Kremer, F. and Bogey, C., "Large-eddy simulation of turbulent channel flow using relaxation filtering: resolution requirement and Reynolds number effects," submitted to *Comput. Fluids*, 2015. See also AIAA Paper 2013-517.

[59]Kim, J., Moin, P., and Moser, R., "Turbulence statistics in fully developed channel flow at low Reynolds number," *J. Fluid Mech.*, Vol. 177, 1987, pp. 133-166.

[60]Spalart, P.R., "Direct simulation of a turbulent boundary layer up to $R_\theta = 1410$," *J. Fluid Mech.*, Vol. 187, 1988, pp. 61-98.

[61]Gloerfelt, X. and Berland, J., "Turbulent boundary layer noise: direct radiation at Mach number 0.5," *J. Fluid Mech.*, Vol. 723, 2012, pp. 318-351.

[62]Bogey, C., Barré, S., Juvé, D., and Bailly, C., "Simulation of a hot coaxial jet : direct noise prediction and flow-acoustics correlations," *Phys. Fluids*, Vol. 21, No. 3, 2009, 035105.

[63]Ahuja, K.K., Tester, B.J., and Tanna, H.K., "Calculation of far field jet noise spectra from near field measurements with true source location," *J. Sound Vib.*, Vol. 116, No. 3, 1987, pp. 415-426.

[64]Viswanathan, K., "Distributions of noise sources in heated and cold jets: are they different?," *Int. J. Aeroacoust.*, Vol. 9, No. 4&5, 2006, pp. 589-626.

[65]Brown, G.L. and Roshko, A., "On density effects and large structure in turbulent mixing layers," *J. Fluid Mech.*, Vol. 64, No. 4, 1974, pp. 775-816.

[66]Arndt, R.E.A, Long, D.F., and Glauser, M.N., "The proper orthogonal decomposition of pressure fluctuations surrounding a turbulent jet," *J. Fluid Mech.*, Vol. 340, 1997, pp. 1-33.

[67]Coiffet, F., Jordan, P., Delville, J., Gervais, Y., and Ricaud, F., "Coherent structures in subsonic jets: a quasi-irrotational source mechanism?," *Int. J. Aeroacoust.*, Vol. 5, No. 1, 2005, pp. 67-89.

[68]Mollo-Christensen, E., Kolpin, M.A., and Martucelli, J.R., "Experiments on jet flows and jet noise far-field spectra and directivity patterns," *J. Fluid Mech.*, Vol. 18, No. 2, 1964, pp. 285-301.

[69]Lush, P.A., "Measurements of subsonic jet noise and comparison with theory," *J. Fluid Mech.*, Vol. 46, No. 3, 1971, pp. 477-500.

[70]Tam, C.K.W., Viswanathan, K., Ahuja, K.K., and Panda, J., "The sources of jet noise: experimental evidence," *J. Fluid Mech.*, Vol. 615, 2008, p. 253-292.

[71]Fernholz, H.H. and Finley, P.J., "The incompressible zero-pressure-gradient turbulent boundary layer: an assessment of the data," *Prog. Aerospace Sci.*, Vol. 32, No. 4, 1996, pp. 245-311.

[72]Tomkins, C.D. and Adrian, R.J., "Energetic spanwise modes in the logarithmic layer of a turbulent boundary layer," *J. Fluid Mech.*, Vol. 545, 2005, pp. 141-162.

[73]Fleury, V., Bailly, C., Jondeau, E., Michard, M., and Juvé, D., "Space-time correlations in two subsonic jets using dual-PIV measurements," *AIAA J.*, Vol. 46, No. 10, 2008, pp. 2498-2509.

[74]Fleury, V., "Superdirectivit 'e, bruit d'appariement et autres contributions au bruit de jet subsonique," PhD Thesis, No. 2006-18, Ecole Centrale de Lyon, Lyon, France, 2006.

[75]Castelain, T., "Contrôle de jet par microjets impactants. Mesure de bruit rayonné et analyse aérodynamique," PhD Thesis, No. 2006-33, Ecole Centrale de Lyon, Lyon, France, 2006.

[76]Bridges, J. and Wernet, M.P., "Validating large-eddy simulation for jet aeroacoustics," *J. Propul. Power*, Vol. 28, No. 2, 2012, pp. 226-234.

[77]Michalke, A., "Survey on jet instability theory," *Prog. Aerospace Sci.*, Vol. 21, 1984, pp. 159-199.

[78]Gutmark, E. and Ho, C.-M., "Preferred modes and the spreading rates of jets," *Phys. Fluids*, Vol. 26, No. 10, 1983, pp. 2932-2938.

[79]Lau, J.C., Morris, P.J., and Fisher, M.J., "Measurements in subsonic and supersonic free jets using a laser velocimeter," *J. Fluid Mech.*, Vol. 93, No. 1, 1979, pp. 1-27.

[80]Arakeri, V.H., Krothapalli, A., Siddavaram, V., Alkislar, M.B., and Lourenco, L., "On the use of microjets to suppress turbulence in a Mach 0.9 axisymmetric jet," *J. Fluid Mech.*, Vol. 490, 2003, pp. 75-98.

[81]Bridges, J., "Effect of heat on space-time correlations in jets," AIAA Paper 2006-2534, 2006.

[82]Bridges, J. and Wernet, M.P., "Effect of temperature on jet velocity spectra," AIAA Paper 2007-3628, 2007.

[83]Bridges, J. and Brown, C.A., "Validation of the small hot jet acoustic rig for aeroacoustics," AIAA Paper 2005-2846, 2005. See also: Brown, C. and Bridges, J., "Small hot jet acoustic rig validation," NASA TM-2006-214234, 2006.